

# EUFAR Summer school, 16-23 April 2008, Utrecht

## Flight mission B359 (22-April-2008)

### Group B Final Report

## 1. Aim and objectives of the flight

Our flight had two main objectives which were based on a number of observations including weather and air quality forecasts. The first was to examine the response of polluted plumes from central Europe to changes in boundary layer stability. Based on the weather forecast it was expected that a south easterly airflow would carry polluted air masses from the industrialised central Europe to the region of the North Sea where the flight would take place. Thus, measurements of horizontal and vertical profiles within the boundary layer were necessary in the area where high concentrations were expected. The second objective was to examine the relationship between aerosol and cloud particle concentrations in cirrus clouds. The cirrus clouds were forecasted to come in front of a frontal system approaching from the west and this seemed an ideal opportunity to examine this relationship.

## 2. The flight preparation phase

### 2.1 Forecast

A number of pre-flight tasks were required. Firstly, it was necessary to prepare our flight plan according to the meteorological conditions in the flight area. Thus a reliable weather forecast was needed. In our case, we observed a high pressure system over Scandinavia and a low pressure over the United Kingdom. A frontal system stretching from North to South and an associated south-easterly airflow were forecast for the day of our flight. These conditions for the time of our flight are shown in [Figures 1 and 2](#).

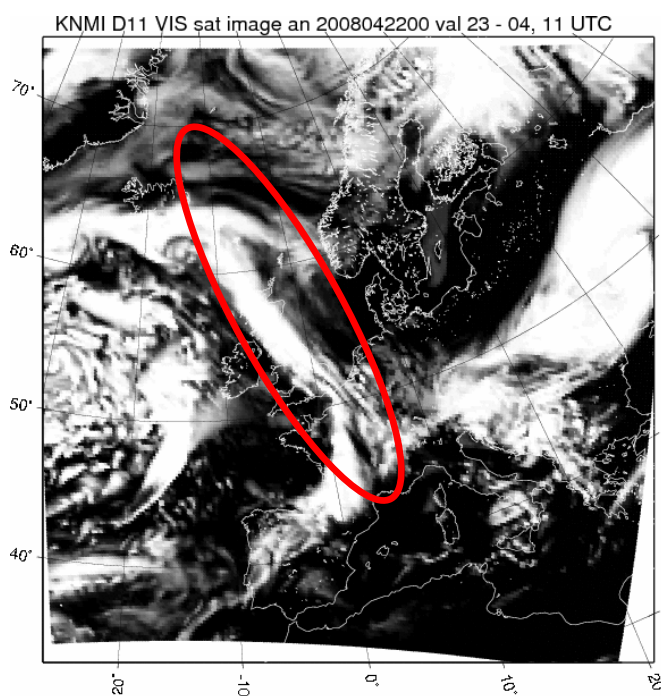


Figure 1. Cloud image from the day of the flight (11 UTC).

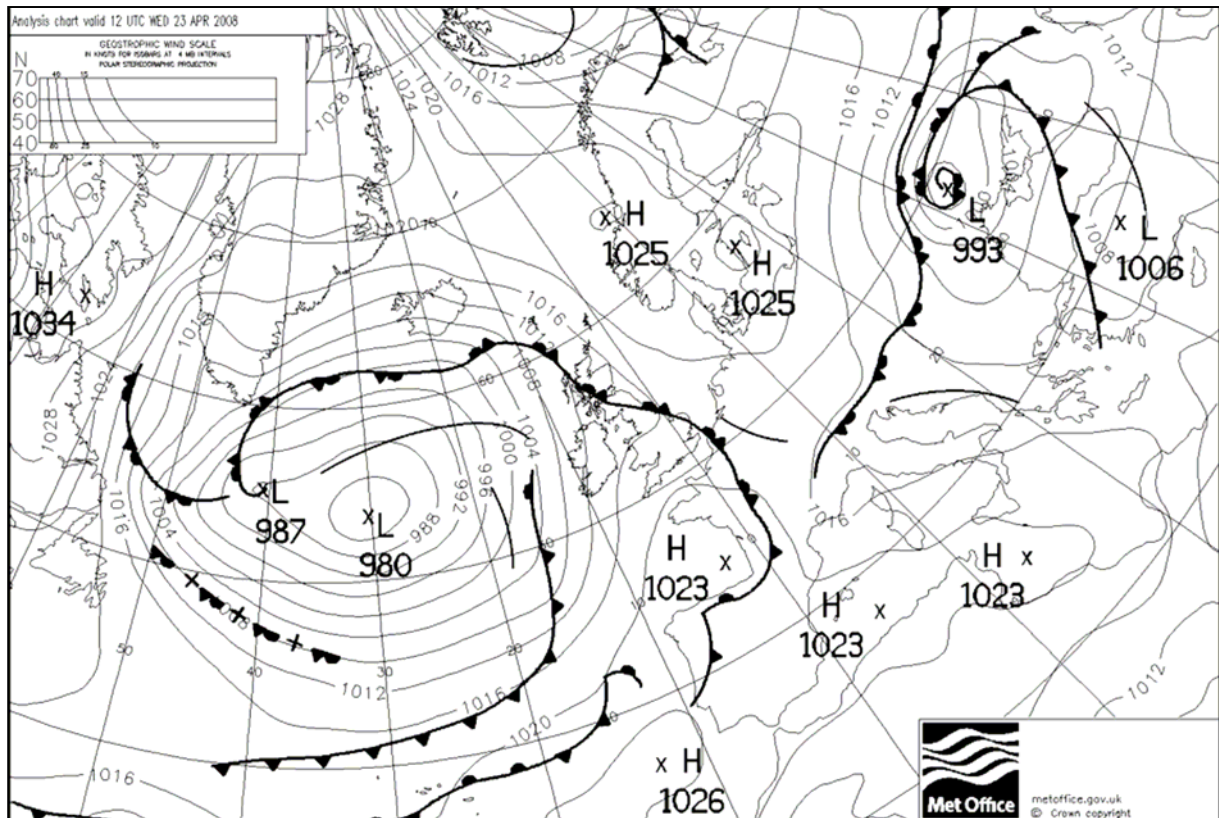


Figure 2. Forecast for the day of the flight (12 UTC).

In addition to the a weather forecast, it was also necessary to have an air quality forecast in order to determine the amount of time to spend within the boundary layer. In the case that low concentrations were expected at low altitudes it would have been wiser to spend more time “hunting clouds” at higher altitudes; this was not the case however. It was expected that polluted air masses from Europe would be carried to our area of interest by the prevailing winds. This was based on back trajectory simulations (Figure 3). More precisely, back trajectories for three different altitudes (500, 1500 and 3000 m) were calculated with HYSPLIT (HYbrid Single-Particle Lagrangian Integrated Trajectory Model) model. It is evident that air masses from the European continent were flowing to our study zone, transporting pollution which would have been characterized by high sulphate and nitrate concentrations.

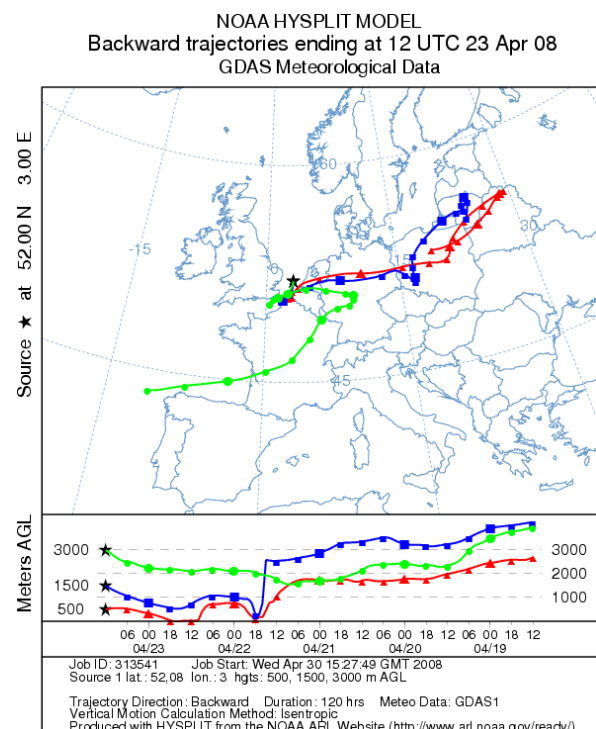


Figure 3. Back trajectory ending at the study zone at 11 UTC for altitude 500, 1500 and 3000 m a.g.l. for 23 April 2008 representing days 19-24.

This was also supported by the NAAPS (Navy Aerosols Analysis and prediction System) sulphate map which showed a high sulphate concentration reaching maximum values in our study zone (Figure 4).

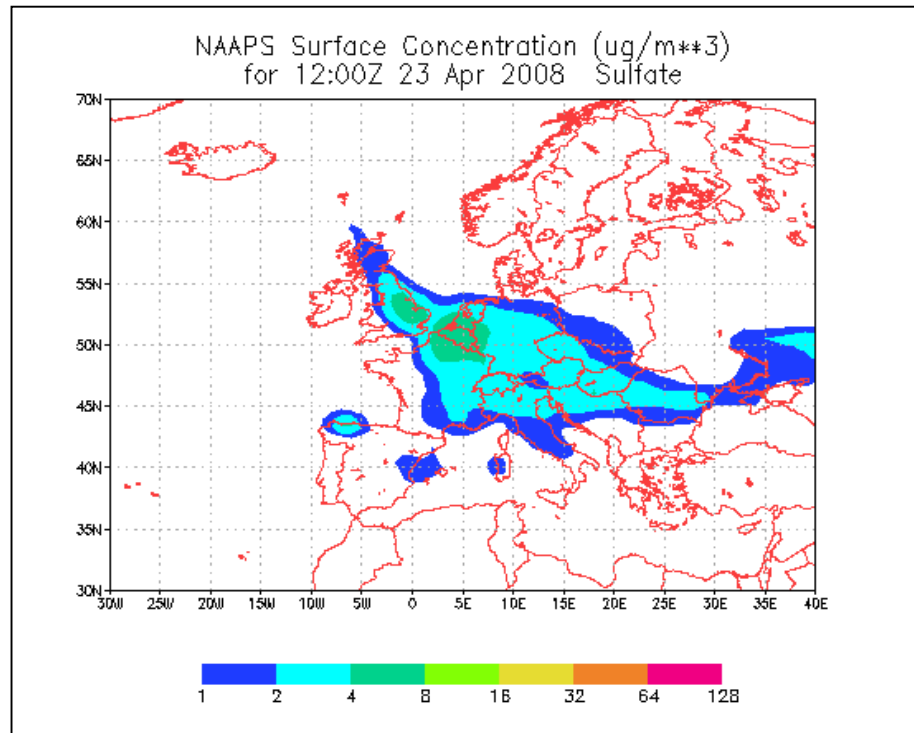


Figure 4. NAAPS surface sulphate concentration ( $\mu\text{g m}^{-3}$ ) map for 23 April 2008 (12:00).

The concentrations were significant enough to warrant spending half of our flight time at low altitudes measuring pollutants concentrations. More particularly it was our belief that particulate matter and sulphur dioxide would be transported from the heavy industrialised areas of the Netherlands and Germany. This primary source of pollution, in addition to the moist air masses that the front would bring to the area of East Anglia and the North Sea would be the basis for the formation of secondary aerosols that would create a high concentration in the locality of our planned flight.

## 2.2 Flight plan

It was then necessary to match our flight objectives with the weather and air quality conditions forecasted. In order to do so, a route was created according to this prediction. Discussion between the students was necessary to prevent time loss during the flight and thus optimize the flying time. To support us, we had Paul's advice and were able to discuss feasible measurements that we could undertake during the flight itinerary.

The flight was structured in two faces. The first was to measure the concentrations of ozone, particulate matter and their respective precursors in the atmosphere (nitrogen oxides for ozone, sulphur oxides for aerosols, etc). The second was to measure properties of clouds and aerosol concentrations in cirrus clouds that we were expect to be present in high altitudes.

One main issue which came out of the discussion was related to the accuracy of the weather forecast. If the weather conditions happened to be different from what we expected, it would be necessary to have alternative plan so that flying time would not be wasted. In our case, the main problem was the formation of cirrus which was uncertain. The second option therefore decided upon was to measure below, inside, and above lower altitude clouds. But even so we still needed an option in the case that the flight was to be cloud free. Indeed the team that had already performed a flight the previous day encountered no clouds at all. So this

option was to measure ship or oil platform plumes and it was based on the fact that this pollution sources are always present in the area.

Once the flight plan was established, a meeting with the pilots was necessary in order to discuss the kind of measurements but also about the area restrictions around the United Kingdom and the North Sea. From that point we discussed about the possible measurement that can be performed in the Dutch airspace. It comes that after the discussion with the pilots, the flight plan were the following:

1. Transit into UK airspace as much as possible with wind direction including one dip to 50ft (1500 ft) (25 mins)
2. Turn perpendicular to plume/wind (10 mins)
3. Dip perpendicular to plume/wind and profile climb to top of boundary layer (15 mins)
4. Climb to FL 300 (15 mins)
5. 4 runs: one below cirrus two in cirrus and one above cirrus (40mins)
6. In final run drop dropsonde
7. Return to base (30 mins)

As mentioned previously, some changes from the initial flight can occur. It was our case, although the changes were not that important, it is worth mentioning them. The first change occurred during the climbing to the cirrus level, where we kept our speed at 1000 feet/min. The second change was the order of the cirrus legs, and also the release of the dropsonde which was made during the first cirrus leg instead of at the ending of the final run. Finally, we did a vertical profile when we started the landing process to Rotterdam Airport.

## 2. Data analysis

### 2.1 Results

After the flight, the data were gathered and analysed. [Figure 4](#) presents the flight route. [Figure 5 and 6](#) presents the altitude for the entire flight based on the aircraft RVSM radar instrument. The first results are presented in [Figure 9](#) and concern carbon monoxide concentrations. One region with high values (red area) and 2 spikes pointed out are noticeable in the diagram. The first region occurs when the aircraft is still on the ground (1<sup>st</sup> set of spikes) as well as until the climb to about 900 meters where the first straight run was performed. The concentrations observed reach 2000 ppb and this is associated with the polluted air of the Rotterdam area (heavily industrialised) and aircraft traffic.

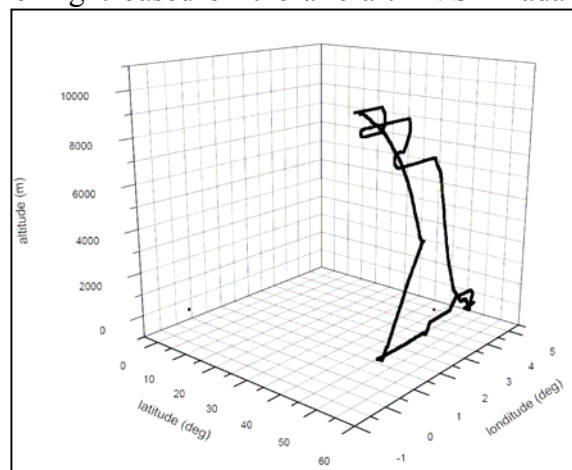


Figure 4. 3D Flight route pattern.

The concentration drops after 900 m to about 500 ppb. Spike 3 is observed during the descent profile back to Rotterdam airport and it is also attributable to local sources. Spike set 1 is observed in the second straight run at 500 m ([Figure 5](#)). This is located at open sea and the spikes coincide with a set of peak presented in NO<sub>x</sub> measurements depicted in [Figure 10](#). The peaks are attributed to ship plumes as these are only anthropogenic pollution source that could generate such short term raise in emissions. Spike set 2 in [Figure 9](#) also coincides with 2

spikes in Figure 10. The first spike of set 2 was observed during the third straight run at 50 ft indicating anthropogenic origin e.g. a ship plume.

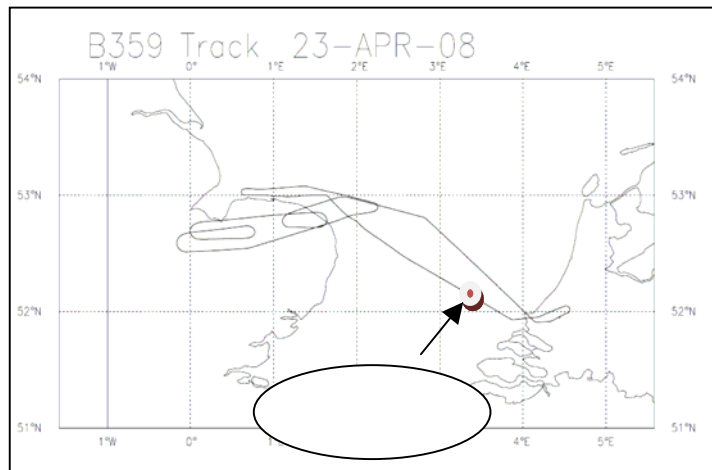


Figure 5. 2D Flight route pattern.

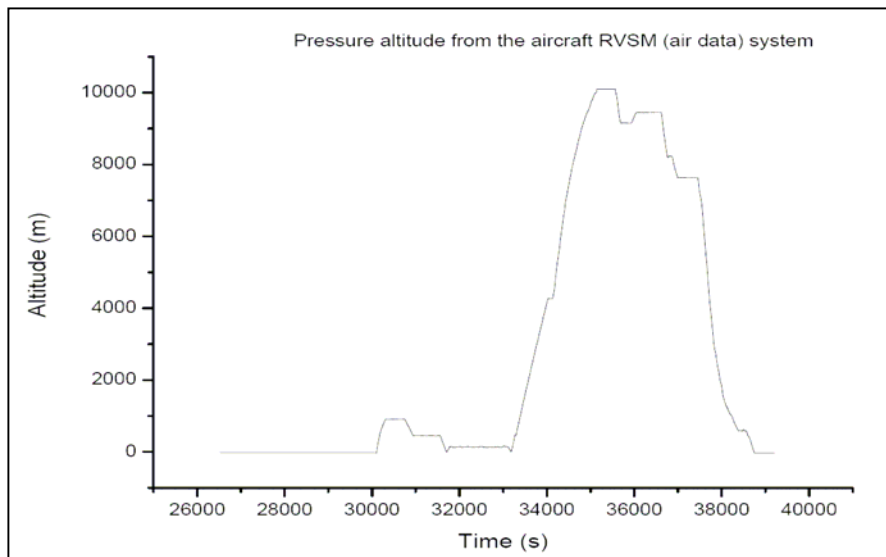


Figure 6. Flight altitude plotted against the actual time.

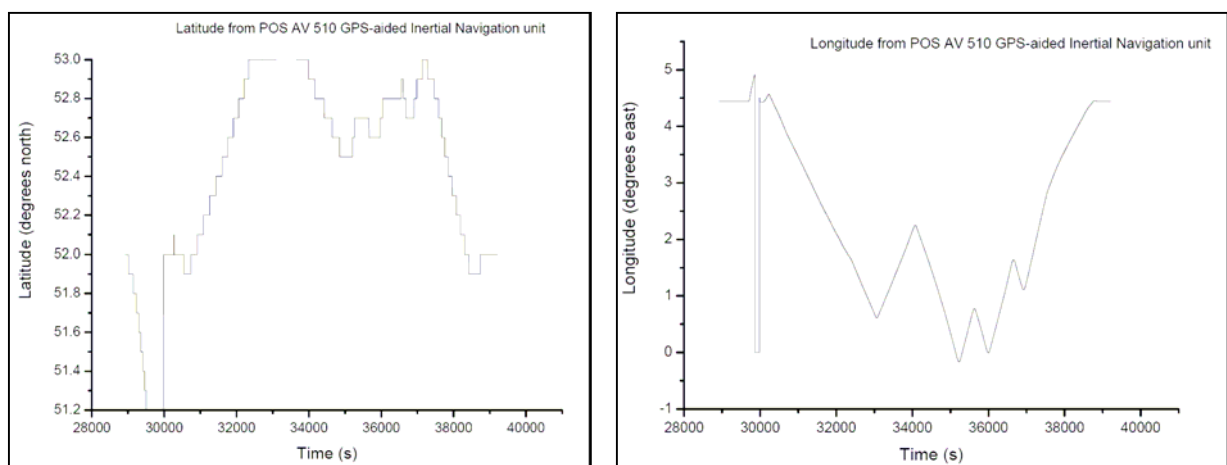


Figure 7. Aircraft position (Lat, Lon coordinates) for the duration of the flight time.

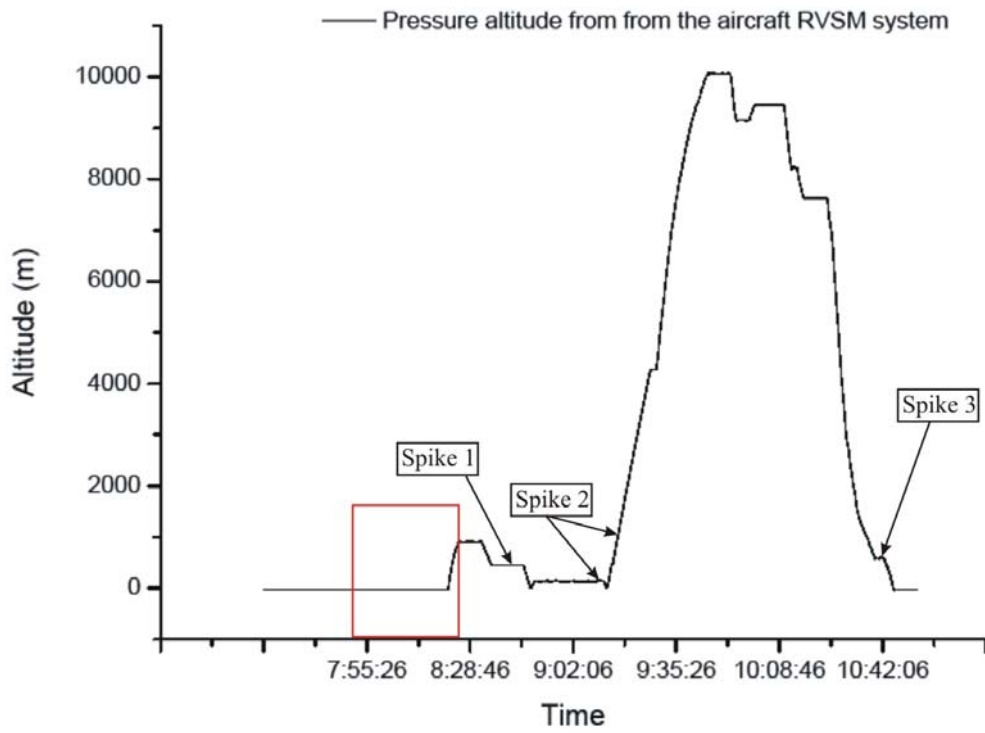


Figure 8. Flight altitude plotted against time written in the NetCDF files showing area of interest.

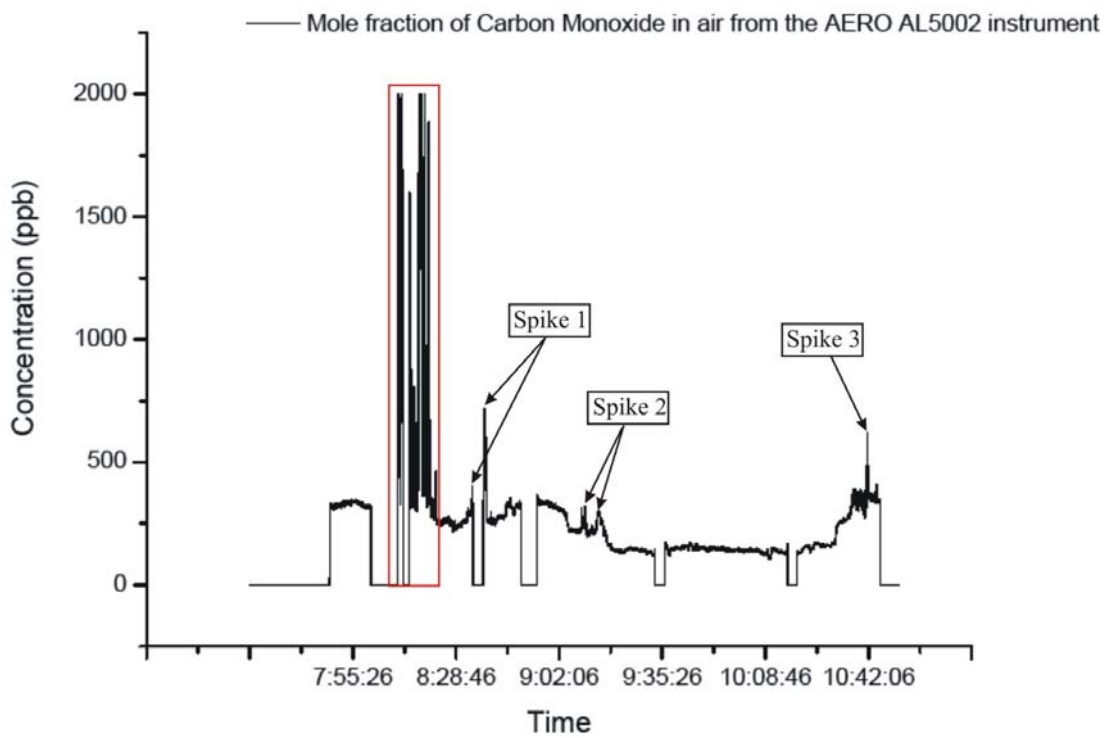


Figure 9. Carbon monoxide concentrations.

The first two regions in NO<sub>x</sub> measurements are within the Rotterdam airport and the peaks are probably due to local sources of the surrounding area. Spike 3 is also attributable to local sources (observed during the profile descent to the airport). Apart from the airport area maxima, the green region in Figure 10 represents the highest concentrations observed during the flight and this is inside the straight run at 50 ft altitude. The latter is considered to be a first indication of transported air pollution from another region to the area of study. The quantity of 50 ppb (measured for duration of more than 15 minutes) is usually observed in polluted urban environments. This is also supported by looking at Figure 11 which presents the wind components. For the duration of the 50 ft straight run, and also before the flight reached this point, a strong northward wind component and a weaker westward component created a northwest wind blowing from continental Europe

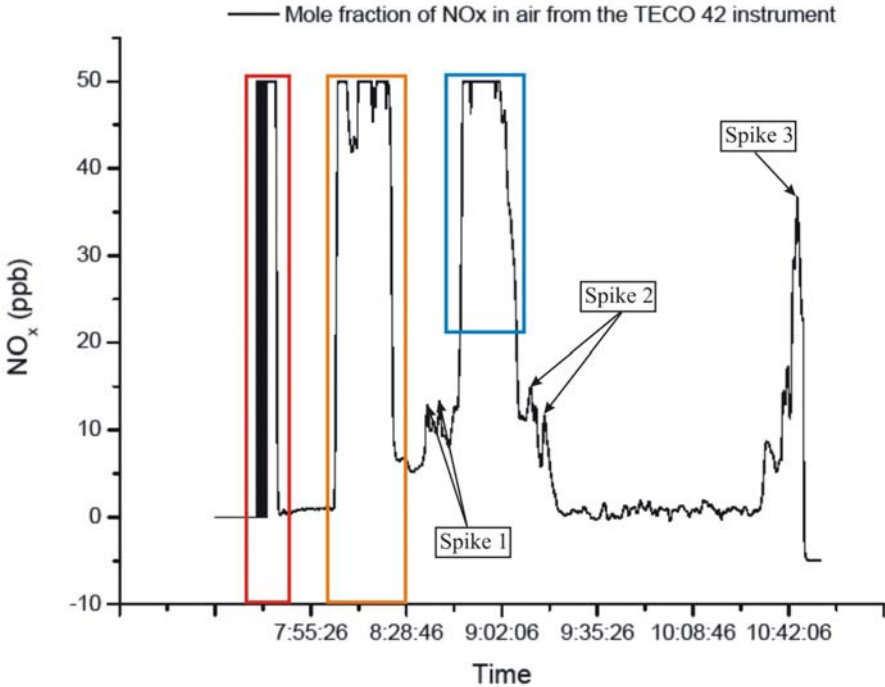


Figure 10. Nitrogen oxides concentrations.

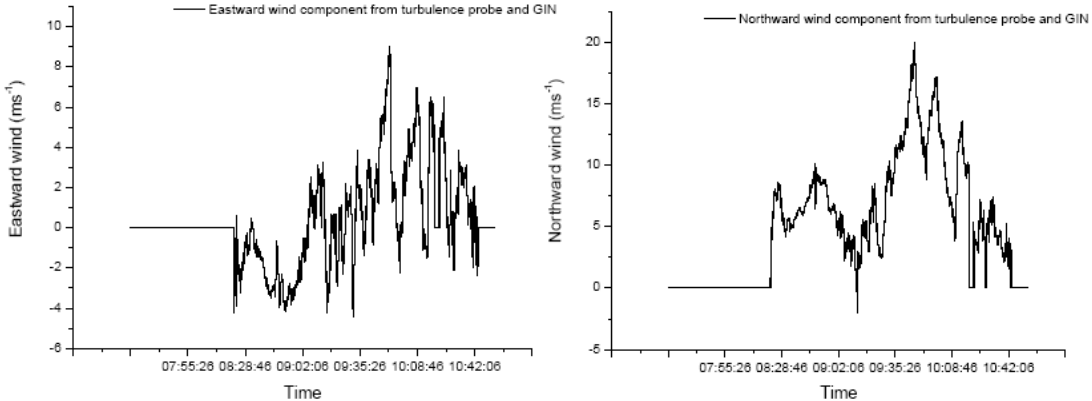


Figure 11. Wind speed components.

The nephelometer is another probe that can be used to assess if whether or not we encountered high concentration of particles. In [Figure 12a](#), we have plotted the scattering coefficient for different wavelengths corresponding to the blue, green and red scattering as a function of the time. In [Figure 12b](#), additional information is given by the backscattering coefficient (also for the 3 wavelengths).

As shown in the figures, the first green blocks correspond to the time when the aircraft were flying 50 feet high above the sea. One would assume that the increased in scattered and backscattered light is associated with the presence of a high amount of sea salt particles.

Then the peak encircled in the red box roughly corresponds to the climbing of the aircraft, reaching a maximum at around 1500 meters (see figure 7), which would correspond to the boundary layer, and at this time of the day, it would be quite probable that the maximum concentration of aerosol is in this height. It is important to mention that above the boundary layer (after the red box), aerosols are rare, explaining why in [Figure 11](#), we have a total scattering and backscattering coefficient of 0 for the time we spent in the high troposphere, hunting for cirrus. The components found are mainly gases (NO<sub>x</sub>, CO, etc...).

Finally the last peaks in the purple boxes correspond again to another run through the boundary layer, but this time during the landing.

One important note is regarding the fact that the nephelometer provides uncorrected data. We do not know if we need to bring any correction or not, but one assumption that can be made from the different values of the scattering coefficient between each wavelengths is that the aerosols encountered had a small size, and that the scattering regime would be the Rayleigh which is dependant of the wavelengths. If this is not the case, then corrections are required.

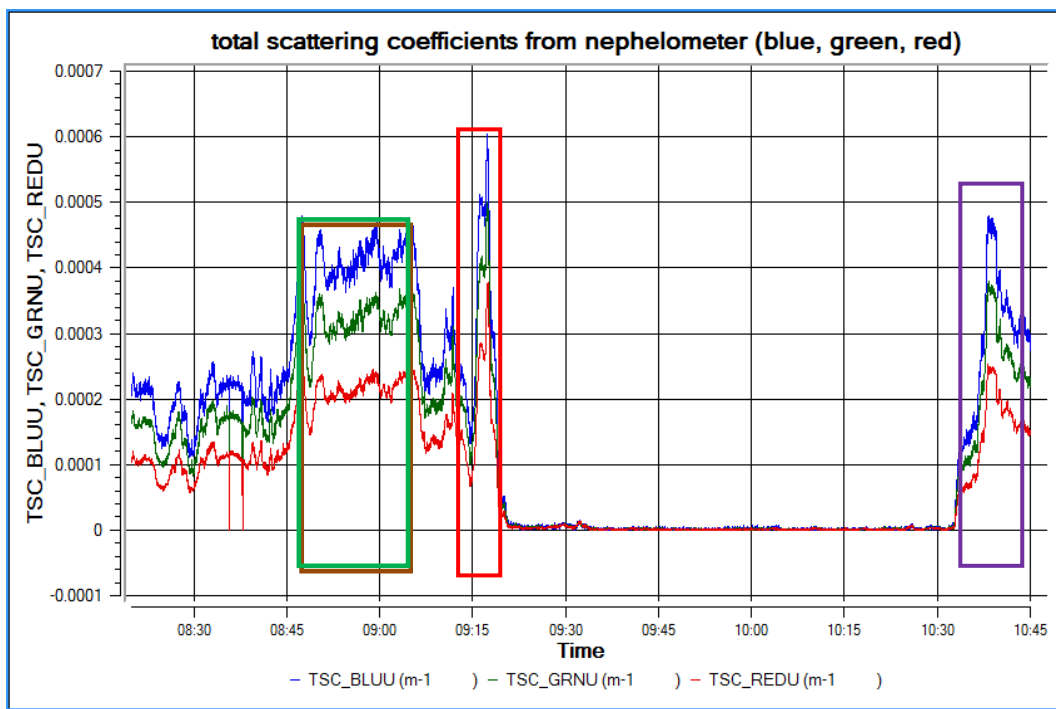


[Figure 12a](#). Scattering coefficient as function of time.



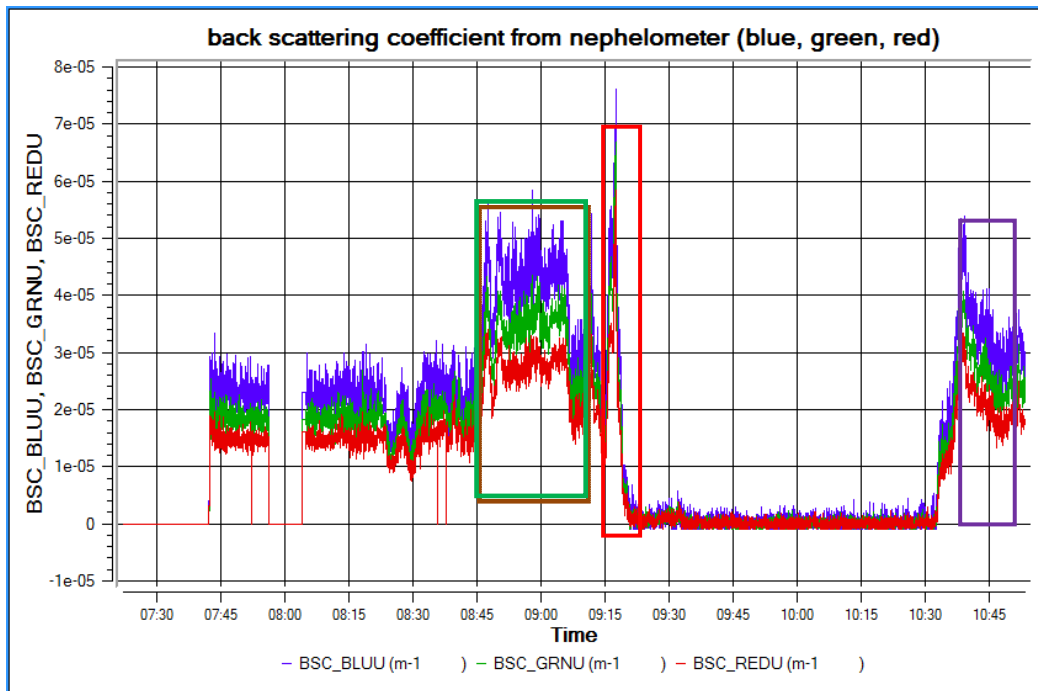


Figure 12b. Backscattering coefficient as function of time.

The second part of the flight was devoted to measurements of cirrus clouds outside the boundary layer. During the flight we encountered cirrus clouds a few times. This is obvious in the time series of cloud particle concentrations measured by the optical array probes (OAP) 2DC and 2DP. The FSSP data are lacking even though there is no failure flag set. Figure 13 shows the concentrations of OAPs along with the flight altitude. Three cirrus encounters are evident. The 2DP measures bigger cloud particles, and therefore, lower concentration than the 2DC. In the time between 09.39 and 10.39h, LWC is displayed in Figure 14. Higher values are observed by the 2DP, again because of the bigger size range of the 2DP probe. Bigger particles contribute more to the LWC.

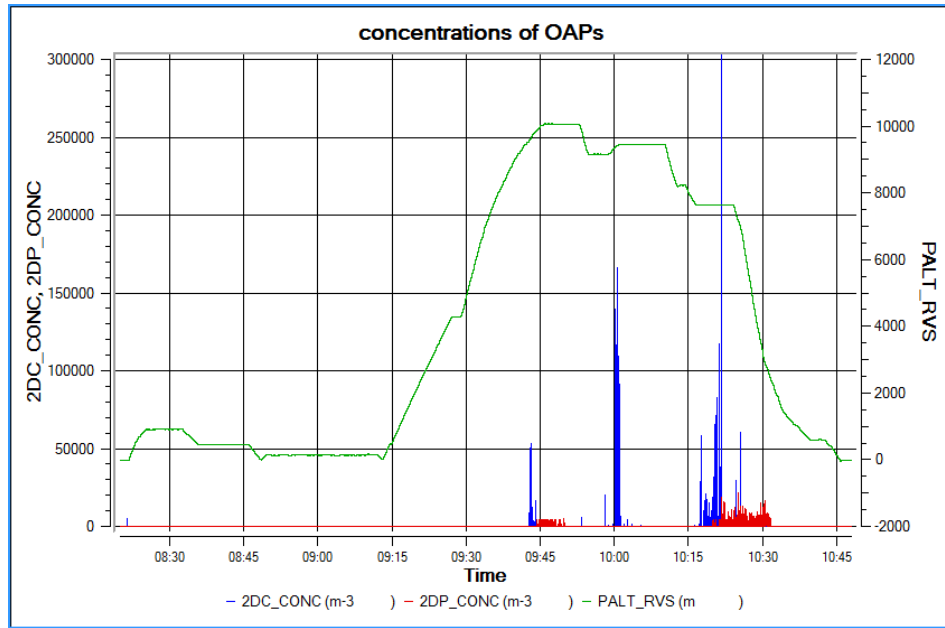


Figure 13. Ice particle concentrations measured with the 2DC and 2DP instruments as function of time.

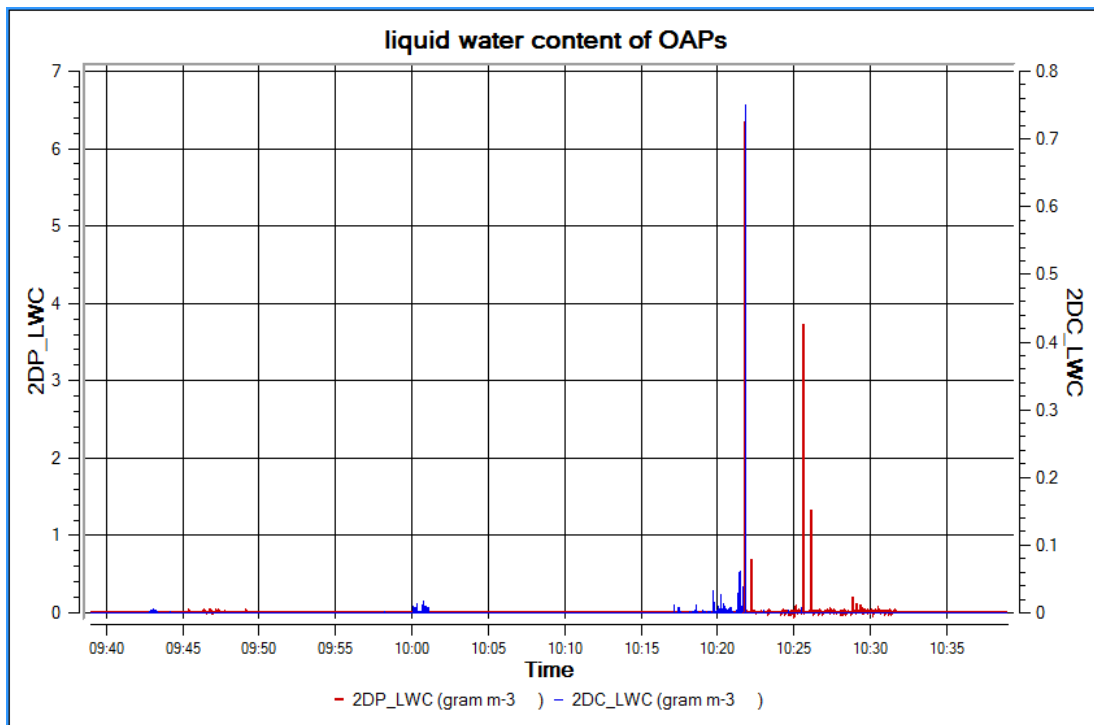


Figure 14. Liquid water content measured with 2DC and 2DP instruments as function of time.

By examining at the PCASP-100 instrument data, particle number concentration evolution - between 0.1 and 3.0  $\mu\text{m}$  - can be studied. In figures 15a and b this evolution has been represented for 2 of the 15 PCASP channels (channel 1 and 8). Particle concentration varies greatly for the studied channels, taking its maximum values in the first of those, which register the smaller particles. Five areas can be emphasized:

- 1- Purple box: during take off operation a polluted layer was found.
- 2- Orange box: corresponds to the 50 feet high above the sea straight run
- 3- The peak found around 9:15 during the climbing of the aircraft, could correspond to the boundary layer. Above the boundary layer, the amount of aerosols in the high troposphere is negligible
- 4- Green box: another polluted layer was found before landing begins
- 5- Blue box: Rotterdam area pollution.

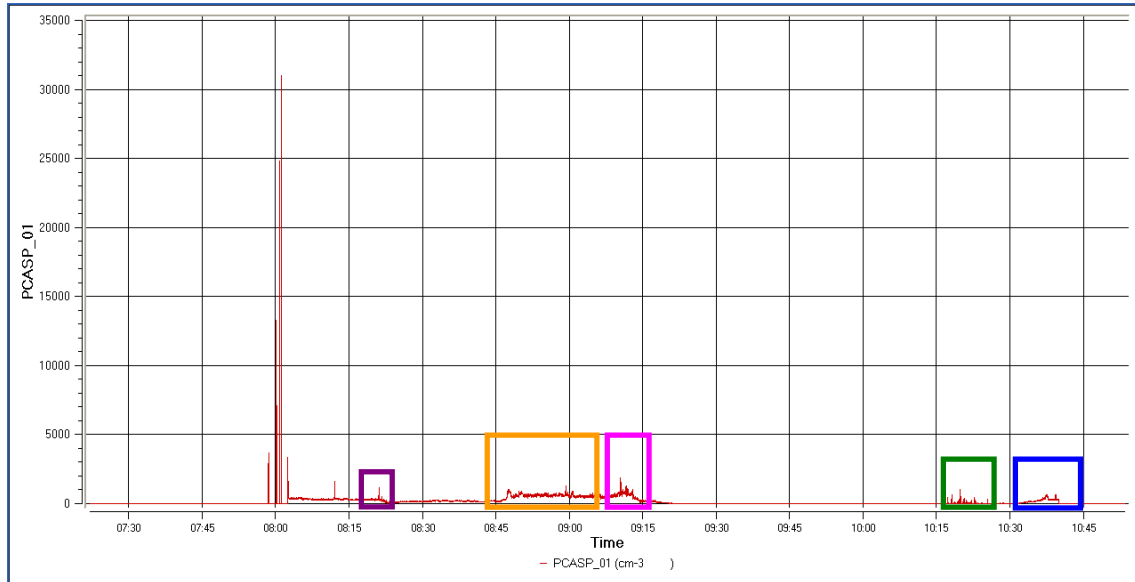


Figure 15a. Particle number concentration from PCASP-100 channel 1 (0.10-0.12  $\mu\text{m}$ ) as function of time (Aircraft take off at 08:22, so important data for us start in this moment).

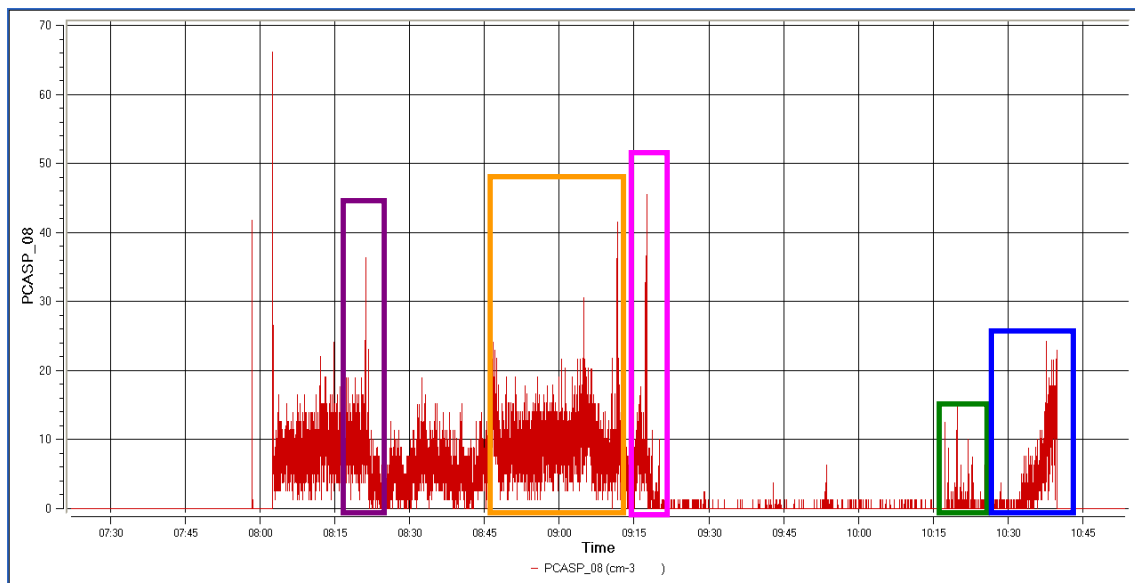


Figure 15b. Particle number concentration from PCASP-100 channel 8 (0.50-0.70  $\mu\text{m}$ ) as function of time.

In Fig. 16, mean concentrations and mean ratio evolutions are depicted. At 08:33 a mean concentration of  $1600 \text{ cm}^{-3}$  was registered. At 08:42, particle concentrations started to increase, reaching between  $2500$  and  $3300 \text{ particles cm}^{-3}$  (time when the aircraft was flying at 50 feet above the sea). At 09:13 a peak of concentration was registered, corresponding to the climbing of the aircraft. This concentration starts to decrease in order to reach a minimum value at 09:23. Concentration is really low until 10:08 (we were in the high troposphere). No more data are available (particles mean concentration during the landing phase are not

available). With respect to mean ratio, it can be seen that at first, a mean value of  $0.11 \mu\text{m}$  was registered. When the maximum concentration was registered, mean ratio was constant ( $0.1 \mu\text{m}$ ). Two peaks in mean ratio were detected, one of them at 09:16 and the other one at 09:31, with values of  $0.16 \mu\text{m}$  and  $0.15 \mu\text{m}$ , respectively. In-cloud nucleation process could be involve in this mean ratio increase.

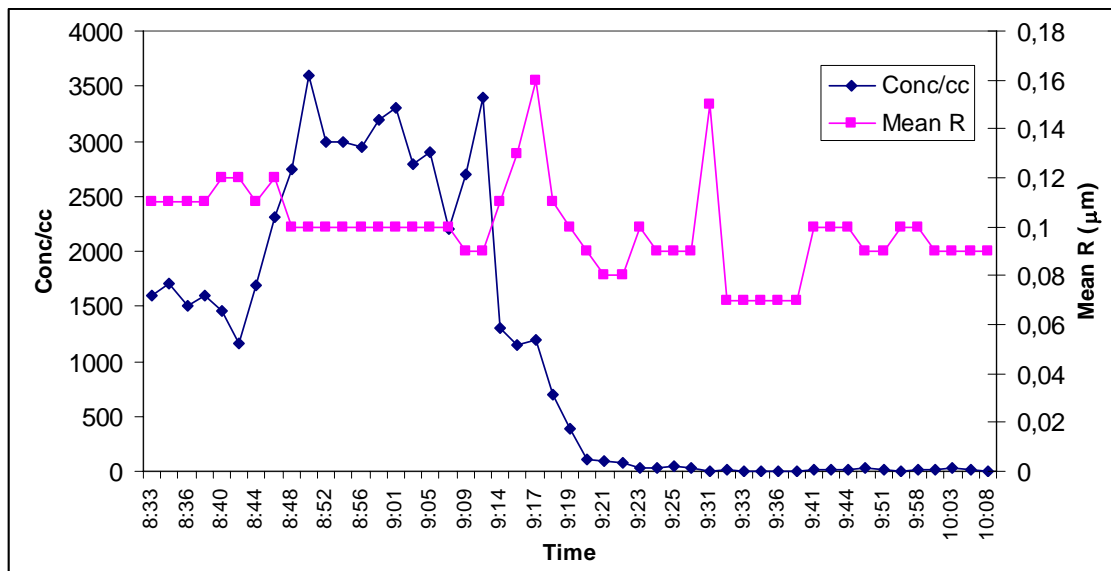


Figure 16. Mean concentration (particles cm<sup>-3</sup>) and mean ratio evolution.

The observed air temperature and dew point temperature are shown at different altitudes in Fig 17a and 17b. Figure 17a shows the vertical profile of temperature values during ascent and Figure 157b shows them during descent. Condensation might have occurred at those altitudes where the two temperature values were same.

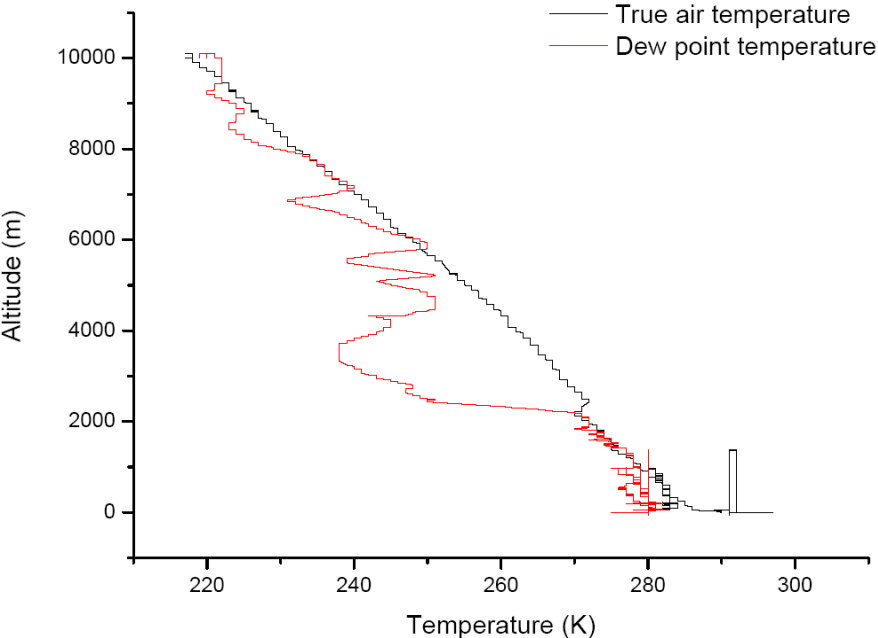


Fig 17a. Vertical profile of true air temperature and dew point temperature during the rise.

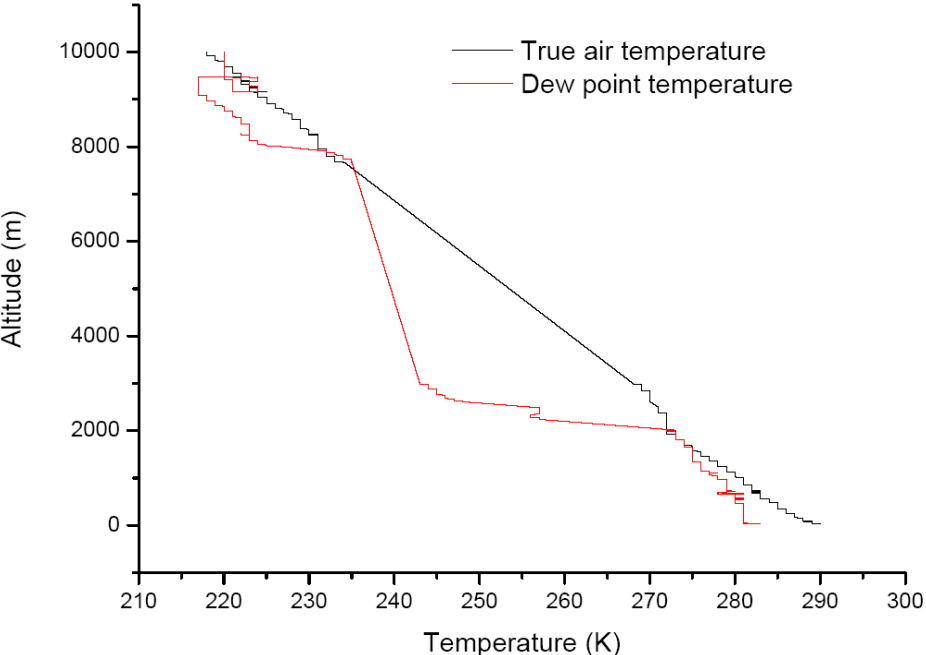


Fig 17b. Vertical profile of true air temperature and dew point temperature during the descent.

The data of upward air velocity were given by turbulence probe and GIN which is seen in Fig 18. Its values contain four spikes. The first and last one of it might be caused by climb and slope. Two strongest downdraft velocities appeared between around between 10:00 and 10:40 when the altitude was between 9000 and 7000 meter. It was around  $-3 \text{ ms}^{-1}$ . In Fig 14 it can be seen that the particle concentrations are the greatest at these altitude.

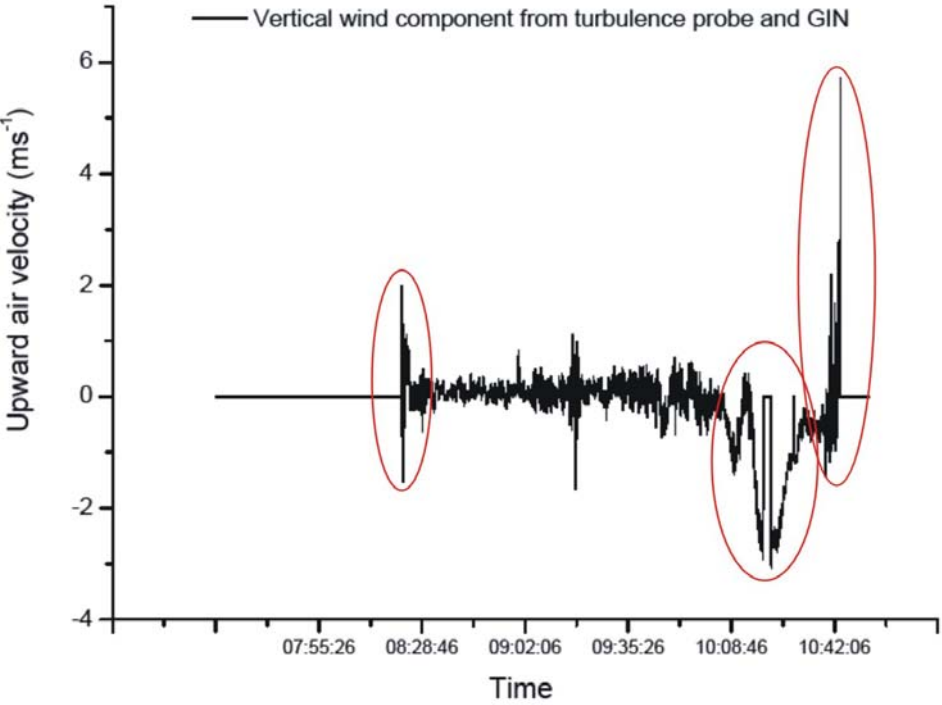


Fig.18 Upward air velocity measured by turbulence probe and GIN.

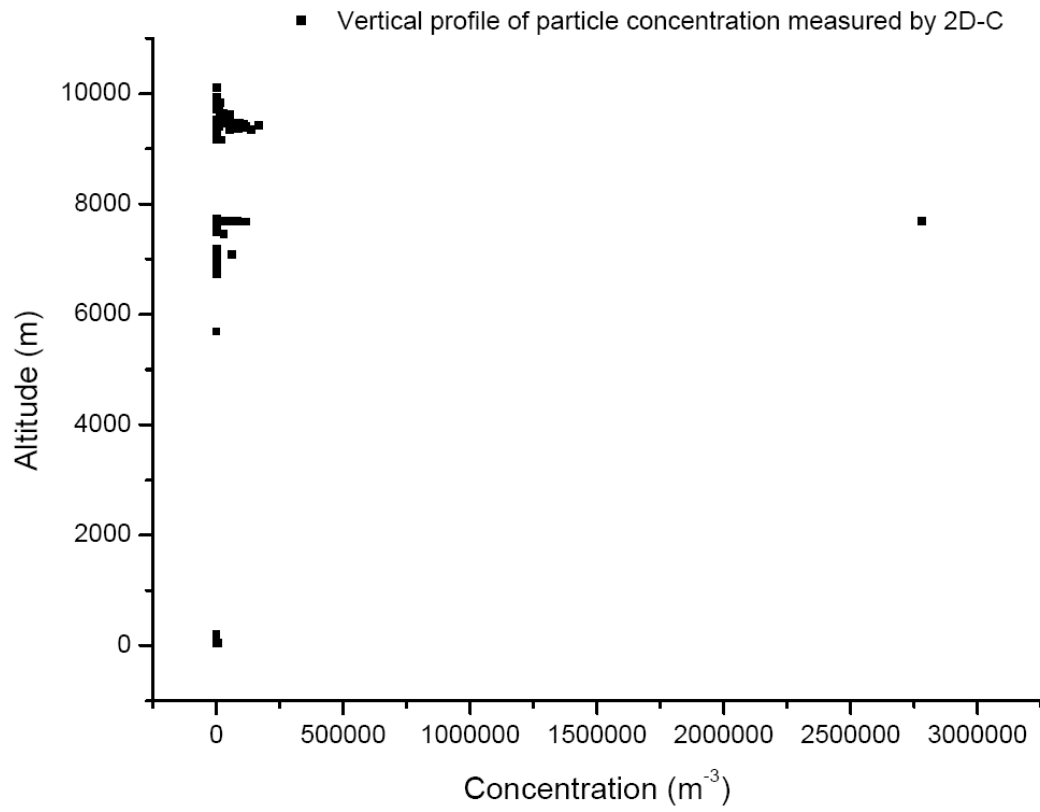


Fig 19a. Vertical profile of particle concentration measured by 2D-C.

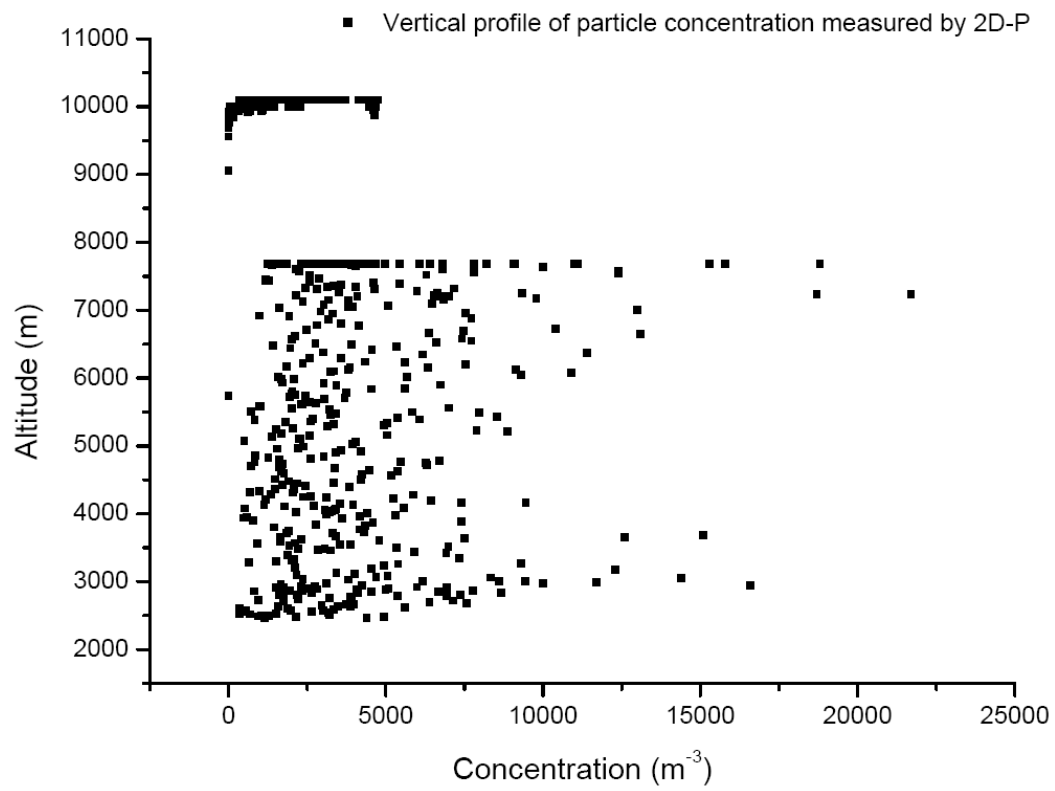


Fig 19b Vertical profile of particle concentration measured by 2D-P.

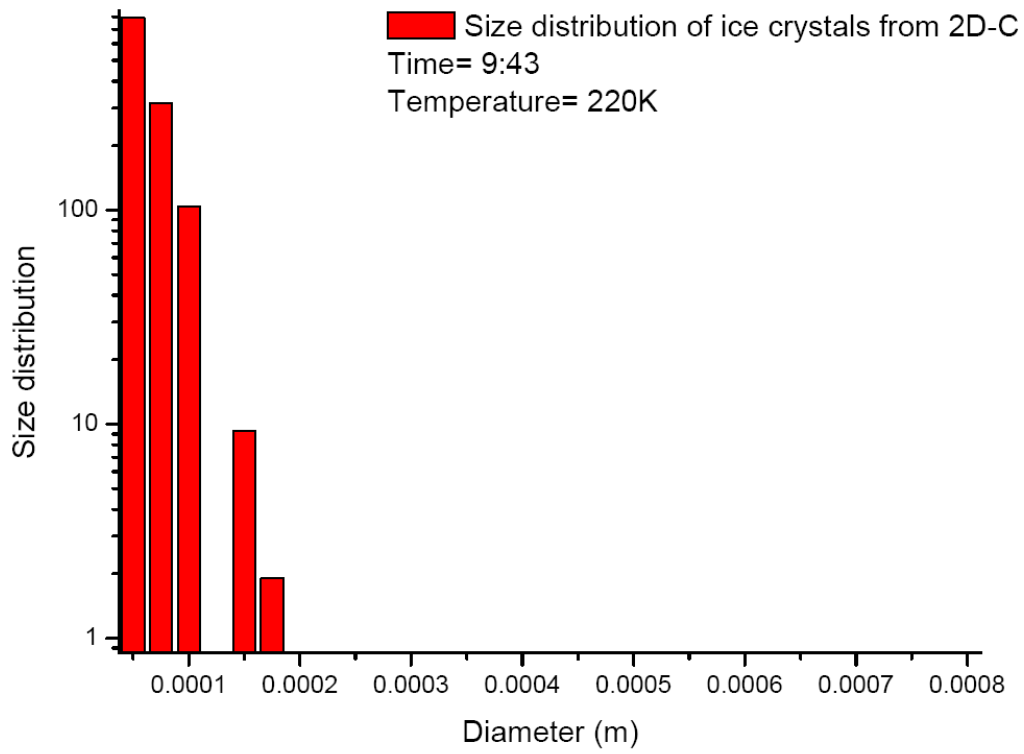


Fig 20.a Size distribution of ice crystals measured by 2D-C at 9:43.

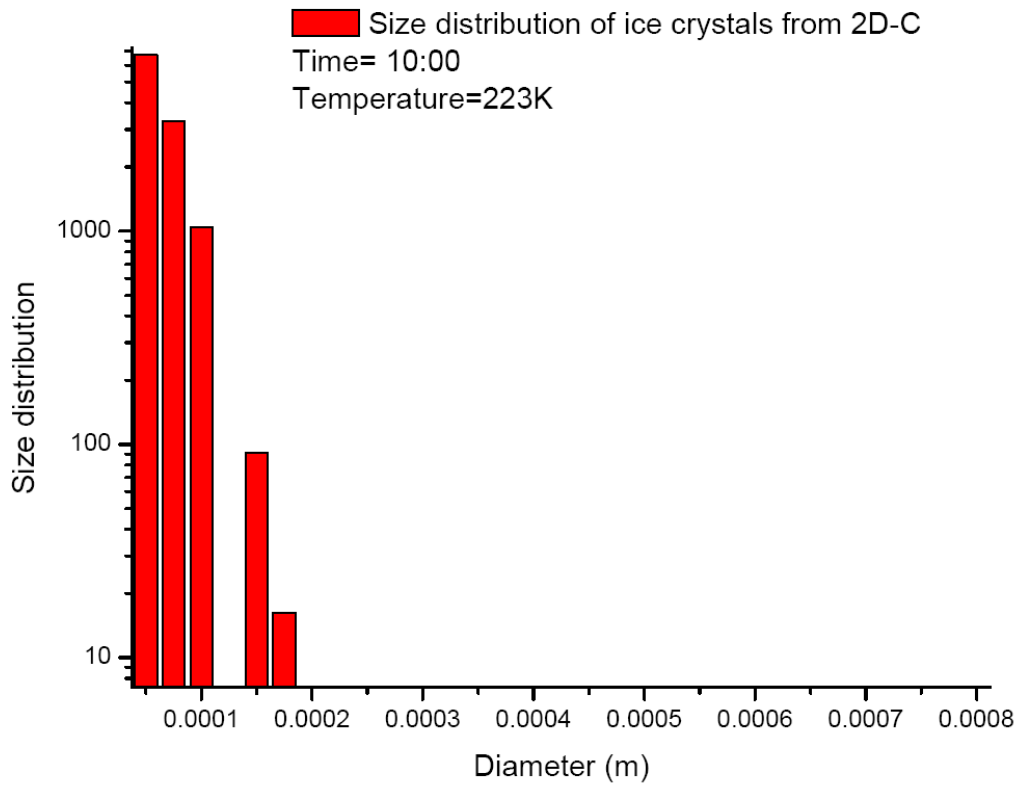


Fig 20b. Size distribution of ice crystals measured by 2D-C at 10:00.



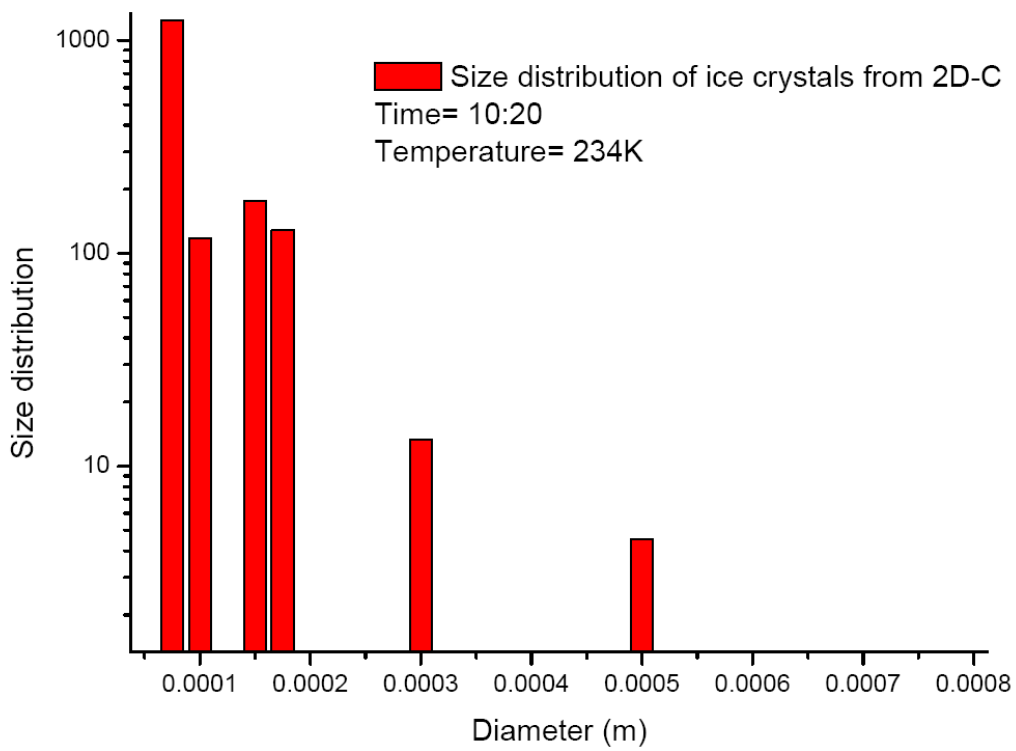


Fig 20.c Size distribution of ice crystals measured by 2D-C at 10:20.

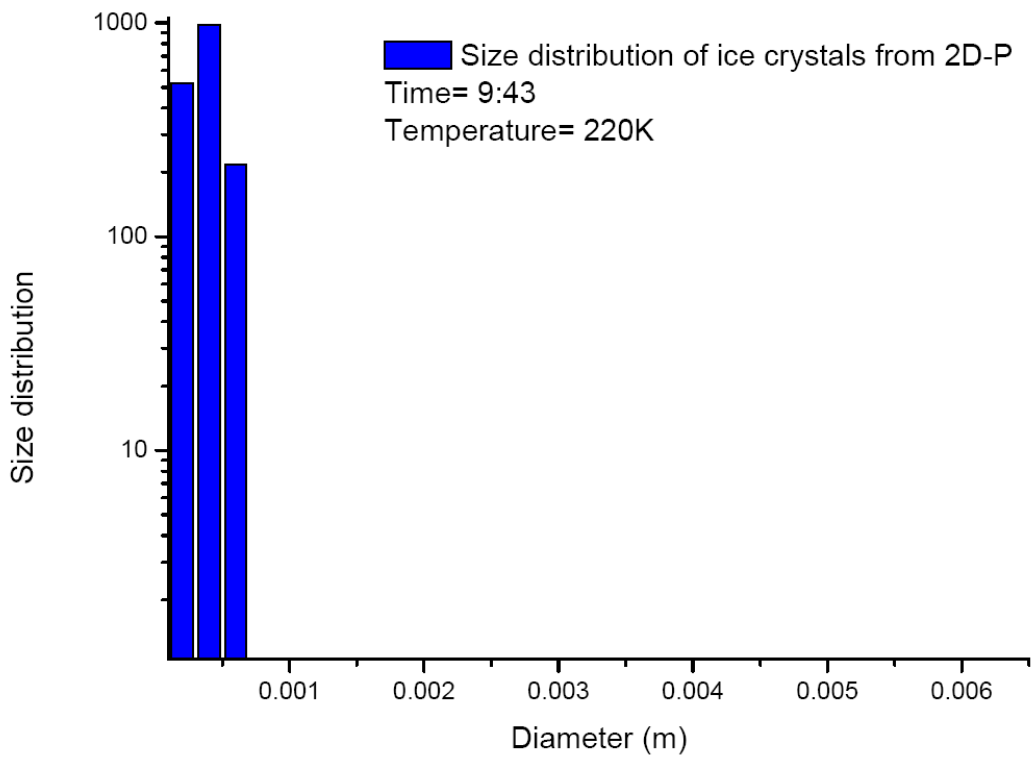


Fig 21.a Size distribution of ice crystals measured by 2D-P at 9:43.

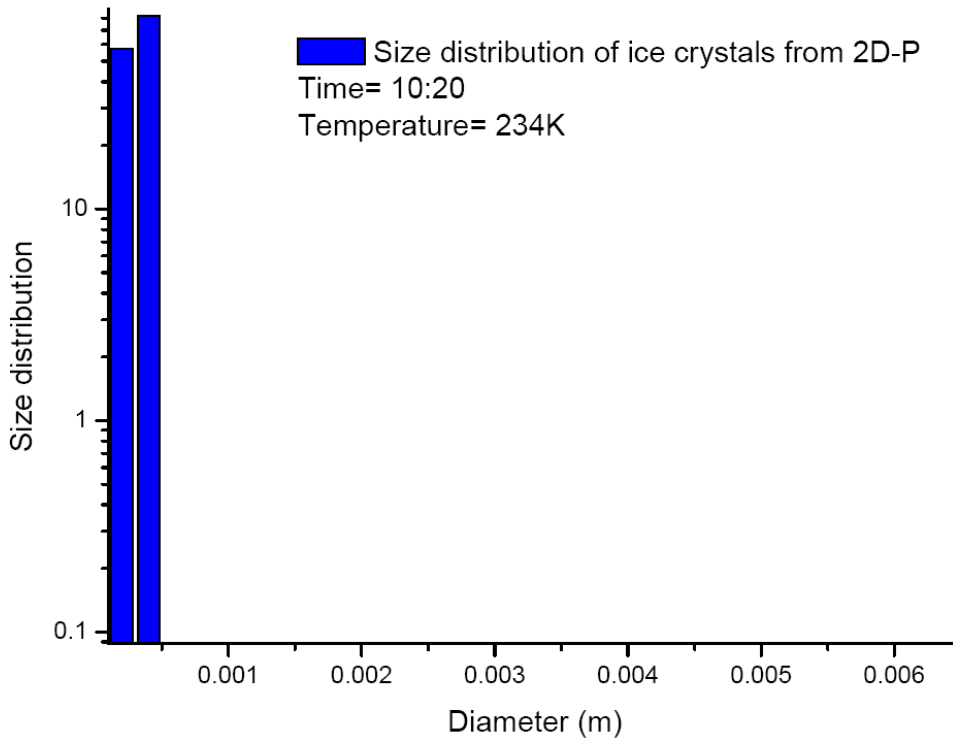


Fig 21.b Size distribution of ice crystals measured by 2D-P at 10:20.

Fig 19a-b shows the vertical profiles of particles concentration measured by 2D-C and 2D-P. The maximum ice particle concentrations were detected in the layer near 8000 m. Limited cloud droplets were also observed near to the surface. The Fig 20ac and 21ab show the size distribution of ice crystals from the 2D-C and 2D-P. The size is given in 32 bins to cover the size range of 25-800  $\mu\text{m}$  diameter with 25  $\mu\text{m}$  resolution in 2D-C and 200-6400  $\mu\text{m}$  diameter with 200  $\mu\text{m}$  resolution in 2D-P. The value of size distribution is given by the following formula:

$$SD = \frac{n_i}{\sum_{i=1}^{i=32} n_i \Delta}$$

Where:  $n_i$  means the concentration values of channels,  $\Delta$  is the width of the bin

The values which were observed by 2DC are given at 9:43, 10:00 and 10:20 when the altitude were 9681 m, 9331 m and 7685 m and the temperature were 220, 223 and 234 K. It can be see that the concentration decreases exponentially with the growth of size in the first two figures. In Figure 20c a reduced concentration decrease is evident (around 100  $\mu\text{m}$ ). In the smaller size range the concentration values were the largest at 10:00, but in the larger size range these were higher at 10:20. The size distributions from 2DP are given at 9:43 and 10:20. Their values were smaller than values which were measured by 2DC.

### 3.2 Description of the instruments

A) *Nephelometer*: In order to measure the scattering coefficient, the integrated nephelometer data was used in our report. The principle consists of measuring the amount of light scattered in all angles by the particles going inside the nephelometer. The light scattering coefficient is given by the following formula:

$$C_{scat}(m, \alpha) = \int_0^{2\pi} \int_0^{\pi} \frac{|S(\theta, \phi)|^2}{k^2} \sin \theta d\theta d\phi ; \quad \sigma_{scat} = \int C_{scat}(m, \alpha) n_N(D_p) d \log D_p$$

S : Angular distribution of scattered light

k : wave number

$\sigma_{scat}$  : scattering coefficient

m : Refractive index

$\alpha$  : size parameter

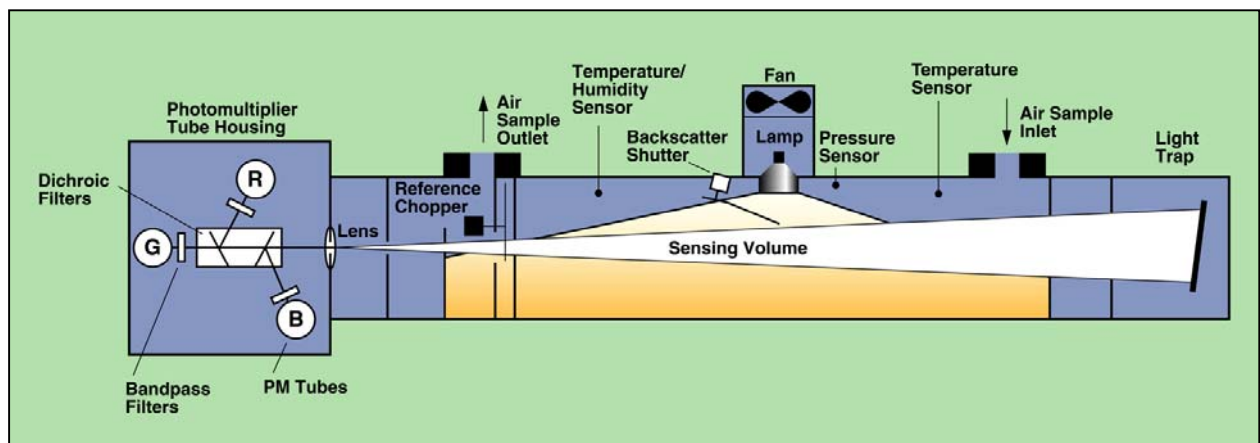
$C_{scat}$  : single particle scattering cross section

$n_N$  : number of particles for each size bins

$D_p$  : Particle diameter

The light scattered is then collected in the different solid angles and then integrated. It is important to mention that the values collected need correction of truncation angles in the forward direction. A schematic of the TSI 3564 nephelometer is depicted in Fig. 22..

Figure 22. Schematic of a Nephelometer.



*B) PCASP-100 (Passive Cavity Aerosol Spectrometer Probe):* is an optical particle counter (OPCs) that detects single particles and size them by measuring the intensity of light that the particle scatters when passing through a Helium Neon laser. Particles that encounter this beam scatter light in all directions and some of this light is collected by a margin mirror over angles from about  $35^\circ$  -  $135^\circ$ . This collected light is focussed onto a photo detector and then amplified, conditioned, digitized and classified into one of fifteen size channels (from 0.1 to  $3.0 \mu\text{m}$ ) (Table 1). The size of the particle is determined by measuring the light scattering intensity, using Mie scattering theory to relate this intensity to the particle size. The size information is sent to the data system where the number of particles in each channel is accumulated over a preselected time period. Usually, this probe is calibrated by the manufacturer using polystyrene latex particles of a known size. The refractive index of latex beads ( $1.59 - 0i$ ) are different from that of atmospheric particles, resulting in an aerosol size distribution that is “latex equivalent”. It is necessary to correct the original size distribution using a refractive index typical of aerosols that are being measured.

Table 1. PCASP-100 Calibration Data Sheet- 0.1 – 3.0  $\mu\text{m}$

| CHANNEL | SIZE( $\mu\text{m}$ ) | INTERVAL( $\mu\text{m}$ ) |
|---------|-----------------------|---------------------------|
| 0       | 0.10 - 0.12           | 0.02                      |
| 1       | 0.12 - 0.14           | 0.02                      |
| 2       | 0.14 - 0.17           | 0.03                      |
| 3       | 0.17 - 0.20           | 0.03                      |
| 4       | 0.20 - 0.25           | 0.05                      |
| 5       | 0.25 - 0.30           | 0.05                      |
| 6       | 0.30 - 0.40           | 0.10                      |
| 7       | 0.40 - 0.50           | 0.10                      |
| 8       | 0.50 - 0.70           | 0.20                      |
| 9       | 0.70 - 0.90           | 0.20                      |
| 10      | 0.90 – 1.20           | 0.30                      |
| 11      | 1.20 – 1.50           | 0.30                      |
| 12      | 1.50 – 2.00           | 0.50                      |
| 13      | 2.00 – 2.50           | 0.50                      |
| 14      | 2.50 – 3.00           | 0.50                      |

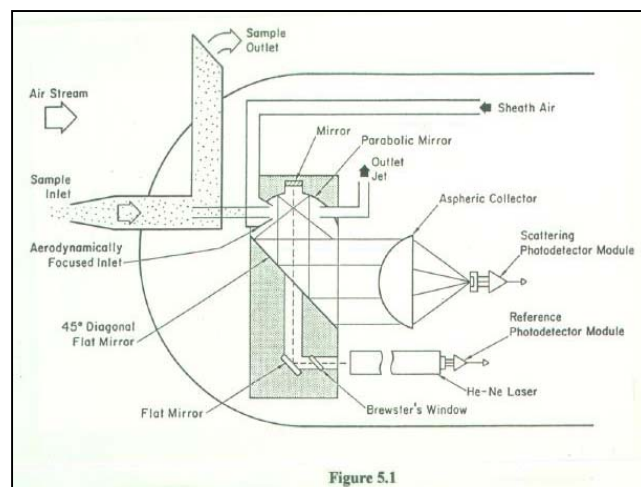
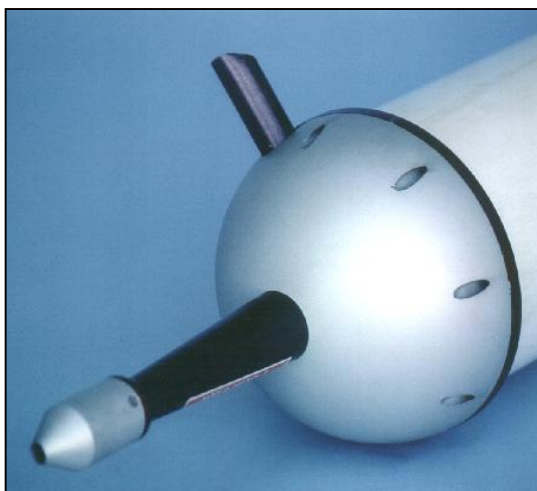


Fig. 23. PCASP-100: a) photograph and b) optical path of this instrument.

*C) Optical Array Probes (2DC and 2DP):* Optical Array Probes (OAPs) measure particle images by capturing the shadow of the particles that pass through a focused laser. Particles cast a shadow on a linear array of diodes (see Figure 17) and the processing electronics record the state of these diodes. The difference between the 2DC and 2DP is the resolution of the diodes and thus, the measured size range. Resolution of the 32 diodes of the 2DC is  $25\mu\text{m}$ , and  $200\mu\text{m}$  for the 2DP, respectively. Thus, size ranges of  $25\text{-}800\mu\text{m}$  (2DC) and  $200\text{-}6400\mu\text{m}$  (2DP) can be observed.

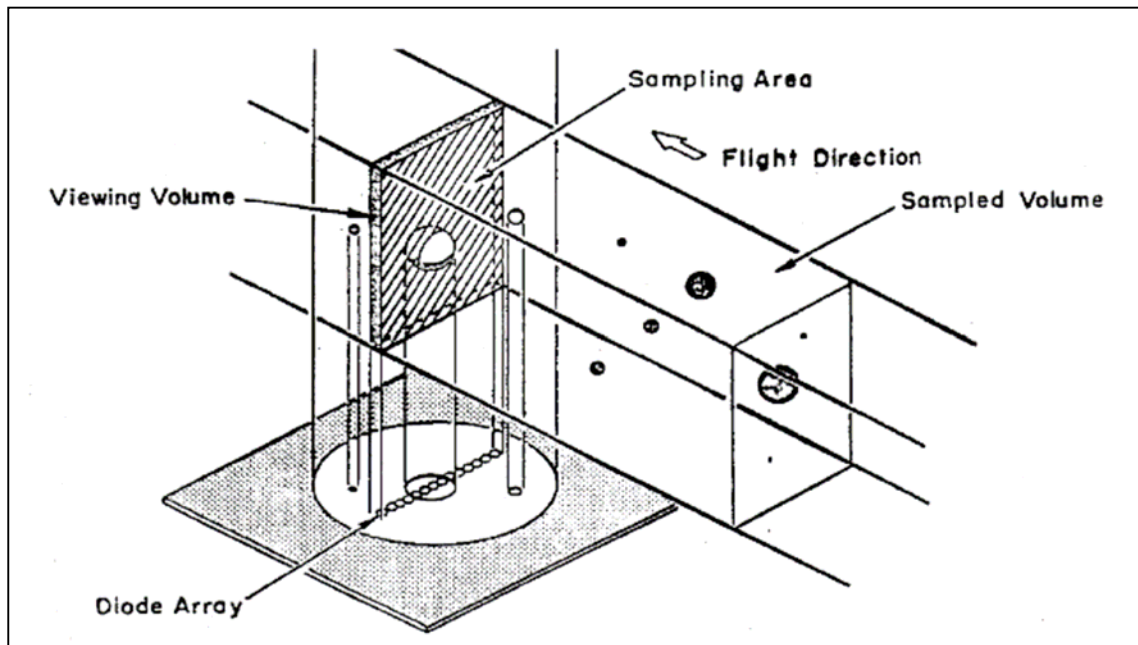


Figure 24. Schematic of Optical array probes 2DP, 2DC.

### 3.3 Main difficulties encountered.

Difficulties encountered were mainly related to data acquisition, and data analysis. Indeed, it was not easy to collect the data as we had a lot of trouble in downloading the data from the FAAM webpage. Data were separated in several files which didn't make it easy to find the results we were interested in. Emails to the different scientists had to be sent in order to get the good path to download the data. The analysis was also chaotic, as we didn't have any appropriate software to analyse them unless re-coding them in Fortran or some other programming languages. We suggest at least for the next summer school, links to some software allowing the students to analyse the data would be useful.